BRITTLE AND DUCTILE FRACTURE TRANSITION IN STEELS SUBJECTED TO MIXED MODE LOADING

T.D. Swankie[1], J.C.W. Davenport[2] and D.J. Smith[1]
1. Department of Mechanical Engineering , University of Bristol, Bristol, U.K., BS8 1TR.
2. Magnox Electric, Berkeley Centre, Berkeley, Gloucestershire, U.K., GL13 9PB.

ABSTRACT

The mixed mode I/II fracture behaviour of two steels, a high strength rotor steel (at room temperature) and a pressure vessel steel (at -120°C) have been investigated using single edge notched specimens. Although fracture was characterised using the mode I and II stress intensity factors (K_I and K_{II}) assuming small scale yielding, both steels exhibited a change in the fracture mechanism with increasing shear loading. In both steels it was found that near mode I fracture occurred by cleavage and with increasing shear, fracture occurred by ductile tearing. The transition in fracture mechanism was found to coincide approximately with the predicted transition from cleavage to ductile fracture.

KEYWORDS

Mixed mode, steels, brittle and ductile transition

INTRODUCTION

Investigations into mixed mode loading have generally been restricted to linear elastic materials since the theoretical analyses (Erdogan and Sih, 1963; Hellen and Blackburn, 1975) are more fully understood than for elastic-plastic materials. For example, the maximum tensile stress (MTS) criterion appears to provide a lower bound to brittle fracture in PMMA (Maccagno and Knott, 1989; Davenport and Smith, 1993) when subjected to combinations of opening (tensile, mode I) and sliding (shear, mode II) loading. The MTS criterion appears also to apply to steels (Yokobori *et al.*, 1983) which fail by transgranular cleavage.

Criteria for elastic-plastic fracture behaviour of materials for combinations of tension and shear are less well developed. Several researchers (Maccagno and Knott, 1991; Davenport and Smith, 1993) suggest that an elastic-hardening plastic analysis (Shih, 1974), combined with the MTS criterion, provides an improved description of mixed mode I/II fracture if brittle fracture occurs under contained yielding. There have been only limited studies to examine the influence of mixed mode loading when ductile fracture occurs. In a steel tested at room

temperature Maccagno and Knott (1992) found that fracture occurred by a localised decohesion mechanism and they suggest that crack tip displacements provide an appropriate characterisation rather than stress intensity factor (K).

The aim of the work presented in this paper was to study circumstances where brittle fracture occurred in tensile loading (mode I), but ductile fracture occurred under shear loading (mode II). A recently developed loading fixture was used to test pre-cracked specimens subjected to combinations of tensile and shear loading. Two steels were examined; a C-Mn pressure vessel steel tested at -120°C and a high strength 3CrMo rotor steel tested at room temperature. The results are compared with earlier studies for brittle and ductile fracture in steels.

EXPERIMENTAL METHODS

Material and Specimens

Two steels were examined; a BS1501-224 Gr490B LT50 C-Mn pressure vessel steel (composition, in wt%, 0.18 C, 1.13 Mn, 0.02 Ni, 0.33 Si, 0.02 Cr, 0.01 V, 0.02 Cu, 0.033 Sb, 0.029 Al, 0.01 Co) and a 3CrMo rotor steel (composition, in wt%: 0.32 C, 0.89 Mn, 0.28 Ni, 0.55 Mo, 3.25 Cr, 0.13 Cu, 0.02 S, 0.033 P, 0.014 Sn, and 0.02 V). For both steels single edge notch (SEN) specimens (fig. 1) were manufactured. There was only limited material for the rotor steel, and specimens were manufactured by electron beam (EB) welding mild steel end pieces onto 20x20x20 mm cubes. Prior to EB welding the cubes were heat treated at 930°C for 30 minutes, quenched in 40% methanol and water, tempered at 300°C for 30 minutes and then allowed to air cool. This produced yield and ultimate tensile strengths of 1295 MPa and 1714 MPa respectively. Because of the very high strength of the rotor steel, relative to the end pieces and the loading fixture (detailed below), the mid-section of each of the welded blanks was machined to provide a waisted SEN specimen as shown in fig. 1. The specimens were not fatigue pre-cracked but notched. The notches were machined in two stages using electro-discharge machining; a starter notch 8mm deep and 0.5mm wide and a final notch 2mm deep and 0.1mm wide thereby producing an a/W ratio equal to 0.5.

The C-Mn pressure vessel steel had yield and tensile strengths of 565 MPa and 708 MPa at -120°C. The SEN specimens were manufactured directly from plate, and fatigue pre-cracked to provide an initial a/W of about 0.5.

Test Fixture and Procedure

Mixed mode I/II loading was applied using a recently developed test fixture (fig. 2) clamped around the SEN specimen. The loading fixture, described in detail elsewhere, (Davenport and Smith, 1993), enables mixed mode I/II loading to be achieved in a standard uniaxial testing machine. When the fixture is loaded through holes 1 pure tensile (mode I) loading of the SEN specimen is achieved. If loaded through holes 6 pure shear (mode II) loading is achieved. Mixed mode conditions are obtained by loading through holes 2, 3, 4 and 5.

All fracture tests were carried out in a servohydraulic test machine under machine displacement control of about 0.5mm/min. The 3CrMo rotor steel was tested at room temperature and the C-Mn pressure vessel steel at -120°C. For the latter tests, an environmental chamber, cooled with liquid nitrogen, was used, with a control thermocouple attached to each specimen. Fourteen tests were carried out for the rotor steel, and 11 tests for the pressure vessel steel.

RESULTS and DISCUSSION

Fracture Toughness

In both steels failure in mode I occurred catastrophically. In mode II there was significant load drop-off prior to final failure. For mixed mode loading there was evidence in the load versus load-line displacement curves of increasing plasticity with an increasing proportion of shear load. Although there was significant plasticity near mode II, the maximum loads P_{max}, sustained by the specimen at or prior to fracture were used to determine linear elastic stress intensity factors, given by

$$K_I = \frac{P_{max}}{B\sqrt{W}} F_I(a/W) \qquad K_{II} = \frac{P_{max}}{B\sqrt{W}} F_{II}(a/W) \tag{1}$$

where B and W are the specimen thickness and width respectively, and $F_I(a/W)$ and $F_{II}(a/W)$ are geometry functions determined by finite element analysis (Davenport and Smith, 1993).

In mode I, the pressure vessel steel exhibited an average toughness K_{If} of 77.8 MPa$\sqrt{m}$ based on 4 tests, and the rotor steel an average toughness of 155 MPa$\sqrt{m}$ based on 2 tests. Here the onset of catastrophic fracture is given the notation K_{If} (for mode I) and K_{IIf} (for mode II) to avoid ambiguity with plane strain definitions of toughness. Examination of the fracture surfaces of the mode I specimens, of both steels, revealed transgranular cleavage fracture.

For combinations of tension and shear the change in the proportion of K_{II}, normalised with respect to the average K_{If}, is shown in fig. 3 as a function of the ratio K_I/K_{If}. The apparent toughness in mode II for both steels was about 60% of the mode I toughness.

For brittle fracture, without the presence of significant near crack tip plasticity, the maximum tangential stress (MTS) criterion of Erdogan and Shih (1963) postulates that the ratios of K_{II}/K_{If} and K_I/K_{If} vary according to

$$\frac{K_I}{K_{If}}\cos^3\left(\theta_0/2\right) - \frac{3}{2}\frac{K_{II}}{K_{If}}\cos\left(\theta_0/2\right)\sin\theta_0 = 1 \tag{2}$$

where θ_0 is the fracture angle that satisfies

$$K_I \sin\theta_0 + K_{II}\left(3\cos\theta_0 - 1\right) = 0 \tag{3}$$

The predicted ratio K_{II}/K_{If} as a function of K_I/K_{If} is shown in fig. 3. Also shown is the predicted ratio assuming that there is near crack tip material hardening. Following Shih (1974), and Budden and Jones (1989), an equivalent MTS criterion for a hardening material is

$$\left(\frac{K_I}{K_{If}}\right)^2+\left(\frac{K_{II}}{K_{If}}\right)^2=\left(\frac{\tilde{\sigma}_{\theta\theta}\{\theta_0,M^p,n\}}{\tilde{\sigma}_{\theta\theta}\{\theta_0,1,n\}}\right)^{-(n+1)}\left(\frac{I_n\{M^p\}}{I_n\{1\}}\right) \quad (4)$$

The dimensionless function $\tilde{\sigma}_{\theta\theta}\{\theta_0, M^p,n\}$ depends on its arguments; the fracture angle θ_0, a near tip mixity parameter M^p (defined by Shih, 1974), and the strain hardening exponent n. The hardening exponent corresponds to the uniaxial stress-strain curve described by $\varepsilon = A\sigma^n$. The dimensionless constant I_n is also a function of M^p. The functions on the right hand side can be determined from graphs provided by Shih, (1974), (see also Maccagno and Knott, 1991). Equation 4 is identical to Eqn. 3 when n=1.

The failure locus, derived from Eqn. 4 for limited hardening with n=2, is shown in fig. 3. Apparently, for $K_I/K_{If} > 0.4$, the mixed mode experimental results for the rotor and the pressure vessel steels lie near to the predicted fracture loci for n=1 and 2. It appears that irrespective of increasing plasticity with increased mixed mode loading, fracture for $K_I/K_{If} > 0.4$ can be adequately described by elastic and small scale yielding MTS criteria. However for $K_I/K_{If} < 0.4$ these criteria would overestimate the failure load. For pure mode II, both steels show toughness' significantly lower than predicted by the elastic and the small scale yielding MTS criteria.

Also shown in fig. 3 are experimental results for a small and large grain sized 1CrMoV steel and En3B steel from Maccagno and Knott (1991). These tests all exhibited cleavage fracture. Although Maccagno and Knott did not illustrate their results in terms of the fracture loci shown in fig. 3, they concluded that by examining the critical tangential fracture stress $\sigma_{\theta\theta c}$, as a function of the degree of near crack tip strain hardening, the MTS criterion can also describe the cleavage fracture in these steels. This is also supported by the results shown in fig. 3, although there is, as with the results for the pressure vessel and rotor steels, significant scatter in the experimental results.

Fracture Faces and Angles

The fracture angle, at the centre of the crack plane for each specimen, was obtained by sectioning each specimen along its length, and one half mounted and polished. The fracture angles, for both steels, are shown in fig. 4 as a function of the equivalent crack angle, β, where

$$\beta = \tan^{-1}\left(\frac{K_I}{K_{II}}\right) \quad (5)$$

In the rotor steel, as with loading at holes 1, fracture at holes 2 and 3 (with β = 82.6° and 73° respectively) occurred by a cleavage mechanism with significant shear lips forming at the edges of the fracture surfaces. At hole 4 (β = 61°) the predominant failure mechanism was shear, although there was evidence of a small amount of cleavage fracture at the centre of the

shear, although there was evidence of a small amount of cleavage fracture at the centre of the crack front. For holes 5 and 6 (β = 38.8° and 0°) the fracture mechanism was entirely shear. The change in mechanism is also evident in the change in fracture angle shown in fig. 4.

For the pressure vessel steel cleavage fracture occurred at holes 1 and 3 (β = 90° and 75.2°). At hole 4 (β = 64.4°) there was ductile tearing of about 150μm directly ahead of the fatigue pre-crack. For distances greater than 150μm, the fracture face was a mixture of dimple and cleavage fracture. At hole 5 (β = 44°) ductile tearing extended to 1.5mm. At larger distances from the crack tip the fracture faces were, again, a mixture of dimple and cleavage fracture. For pure shear (hole 6, β = 0°) the fracture mechanism was entirely shear.

The predicted variation of θ_0 according to the MTS criterion (Eqn. 3) is shown in fig. 4. The prediction for θ_0 when n=2 is almost identical to that for n=1. Also shown in fig. 4 are the measured fracture angles from the small and large grained 1CrMoV and En3B steels examined by Maccagno and Knott (1991). Their results illustrate good agreement with the MTS criterion. Certainly at holes 2 and 3 (β > 70°) the measured angles for cleavage fracture in the rotor and the pressure vessel steels agree with the MTS criterion. However, for greater amounts of shear loading, (β < 70°), the fracture angles for the rotor steel deviate significantly from the MTS criterion. This is not surprising since it was observed that the fracture mechanism was not cleavage but a shear mechanism. In the pressure vessel steel there was not significant deviation from the MTS criterion until β < 50°. The fracture faces for 40° < β < 70° from the pressure vessel steel tests showed combined dimple and cleavage fracture.

For failure by a shear decohesion mechanism Maccagno and Knott (1992) suggest that a maximum shear stress criterion $\sigma_{r\theta}$ is appropriate. This hypothesis is supported by their room temperature results for fracture by shear in a lightly tempered HY130 steel. There was considerable plasticity exhibited in the load-displacement curves for these tests. This is similar to the observations from the rotor and the pressure vessel steels for significant amounts of shear loading. The fracture angles for the HY130 tests are shown in fig. 4. There is a similar trend to the results for the rotor steel when the equivalent crack angles β are less than about 60°.

For shear fracture, near-tip slip line field analyses (Shih, 1974; Budden, 1987, 1988), suggest that the angle of maximum shear stress (and strain) for plane strain conditions ranges from 90° for mode I to 0° for mode II. Alternatively for extensive plasticity the direction of the maximum extent of the plastic zone provides an indication of the direction of the ductile tearing. The predicted directions (θ) of the plastic zones obtained by Budden (1988) are shown in fig. 4 as a function of equivalent crack angle β. The curves for the MTS criterion and the direction of the maximum extent of the plastic zone coincide at β = 70°. The transition from brittle to ductile fracture in the rotor steel appears to also coincide at about 70°. There was also evidence of ductile tearing (albeit small) in the pressure vessel steel at β = 64.4°. The transition between brittle and ductile fracture in both steels coincides approximately with the predicted transition from a maximum tensile stress to a ductile shear failure mechanism.

Earlier, Maccagno and Knott (1991) also found that in a C-Mn steel tested at -196°C there was evidence of ductile tearing prior to cleavage fracture. However, their measured fracture angles did not deviate significantly from the MTS criterion. Nevertheless, the transition from

brittle to ductile fracture was explained in terms of the reduced constraint introduced by crack tip blunting. This reduces the near tip stress such that the critical stress $\sigma_{\theta 0c}$ is not achieved. For the rotor steel and the pressure vessel steel the fracture faces and angles illustrate that for $\beta > 70°$ ($K_{II}/K_I < 0.36$) fracture was controlled by a critical stress criterion (MTS). This also corresponds to $K_{II}/K_{If} < 0.36$ in fig. 3. However, the experimental results shown in fig. 3 illustrate there was reasonable agreement with the elastic and elastic-plastic MTS criteria for $K_{II}/K_{If} < 0.6$. The results shown in fig. 4 do not support this. The agreement between experimental results and predictions for $K_{II}/K_{If} < 0.6$ in fig. 3 is therefore misleading.

CONCLUSIONS

1. A 3CrMo high strength rotor steel, tested at room temperature, and a C-Mn pressure vessel steel, tested at -120°C, were found to exhibit a brittle to ductile fracture transition when subjected to mixed mode loading.

2. Mixed mode fracture toughness expressed in terms of stress intensity factor were found to agree with the elastic and small scale yielding MTS criteria for $K_{II}/K_I < 1$. For $K_{II}/K_I > 1$ these criteria would overestimate the failure load.

3. The fracture mechanism was found to change from cleavage to ductile fracture at about $K_{II}/K_I < 0.36$. The predicted change from brittle to ductile fracture was found to agree approximately with the experimental fracture transition.

Acknowledgements - The financial sponsorship for this work was provided by EPSRC, grant numbers GR/F57922 and GR/K21894, Nuclear Electric plc and TWI.

REFERENCES

Budden, P. J. (1987). The stress field near a blunting crack tip under mixed modes 1 and 2. *J. Mech. Phys. Solids*, **35**, 4, 457-478.

Budden, P. J. (1988). The effect of blunting on the strain field at a crack tip under mixed modes 1 and 2. *J. Mech. Phys. Solids*, **36**, 5, 503-518.

Budden, P. J. and Jones, M. R. (1989). Mixed mode fracture. *CEGB Research report,* RD/B/6159/R89.

Davenport, J. C. W. and Smith, D. J. (1993). A study of superimposed fracture modes I, II and III on PMMA. *Fat. Fract. Engng. Mater. Struct.*, **16**, 10, 1125-1133.

Erdogan, F. and Sih, G. C. (1963). On the crack extension in plates under plane loading and transverse shear. *J. Basic Engng.*, **85D**, 519-525.

Hellen, T. K. and Blackburn, W. S. (1975). The calculation of stress intensity factors for combined tensile and shear loading. *Int. J. Fract.*, **11**, 605-617.

Maccagno, T.M. and Knott J. F. (1989). The fracture behaviour of PMMA in mixed modes I and II. *Eng. Fract. Mech.*, **34**, 65-86.

Maccagno, T. M. and Knott, J. F. (1991). The low temperature brittle fracture behaviour of steel in mixed modes I and II. *Eng. Fract. Mech.*, **38**, 2/3, 111-128.

Maccagno, T. M. and Knott, J. F. (1992). The mixed mode I/II fracture behaviour of lightly tempered HY130 steel at room temperature. *Eng. Fract. Mech.*, **41**, 6, 235-252.

Shih, C. F. (1974). Small scale yielding analysis of mixed mode plane strain crack problems. *Fracture Analysis*, ASTM STP **560**, 187-210.

Yokobori, T., Yokobori, A. T., Sato, K. and Omotami, M. (1983). The effects of ferrite grain size on fracture of low carbon steels under mixed modes I and II. *Eng. Fract. Mech.*, **17**, 75-85.

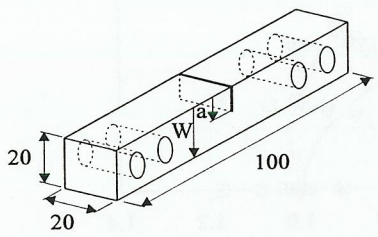

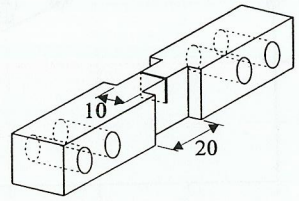

a/W=0.5
All Dimensions in mm

Fig. 1a, Single Edge Notch (SEN) Specimen.

Fig. 1b, Waisted Single Edge Notch (SEN) Specimen.

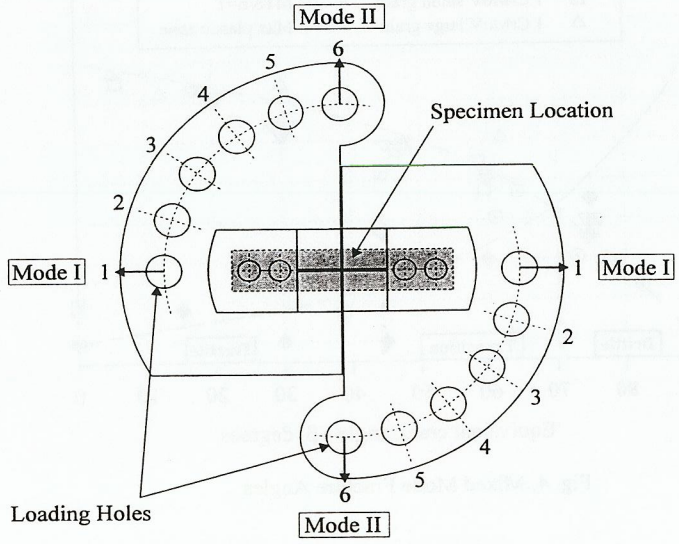

Fig. 2, Mixed Mode I/II Testing Fixture.

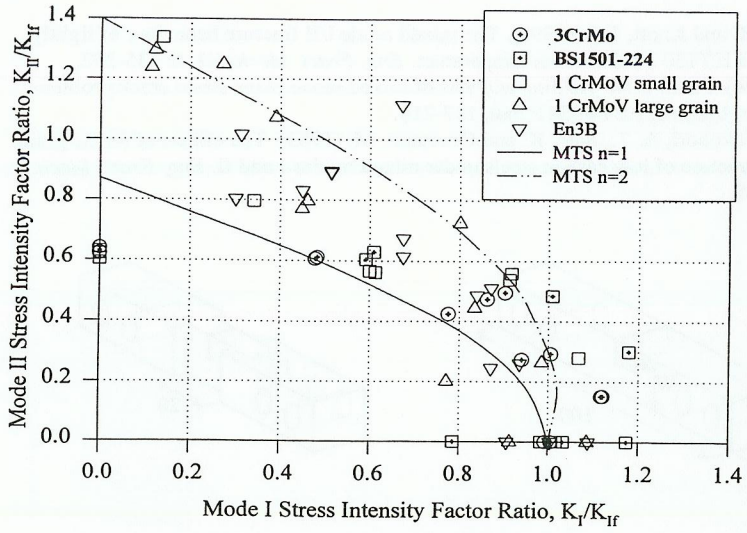

Fig. 3, Mixed Mode Fracture Toughness

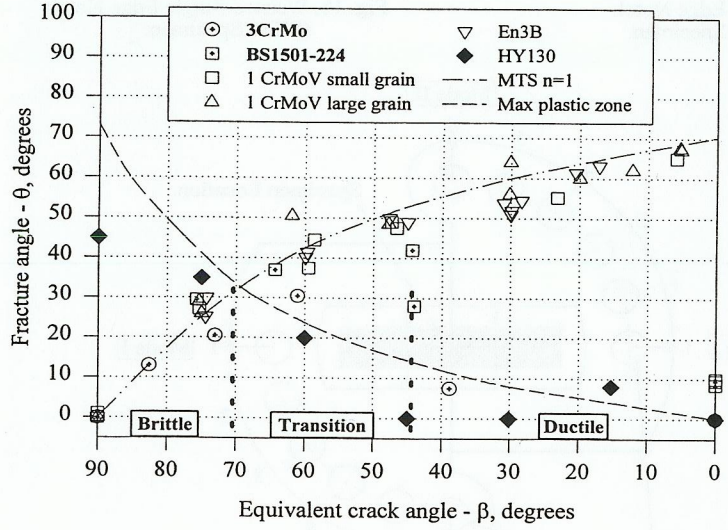

Fig. 4, Mixed Mode Fracture Angles